





Article

Unusually Small Thermal Expansion of Ordered Perovskite Oxide $\text{CaCu}_3\text{Ru}_4\text{O}_{12}$ with High Conductivity

Akihiro Tsuruta ^{1,*}, Katsuhiko Nomura ¹, Masashi Mikami ¹, Yoshiaki Kinemuchi ¹,
Ichiro Terasaki ^{1,2}, Norimitsu Murayama ³ and Woosuck Shin ¹

¹ National Institute of Advanced Industrial Science and Technology (AIST), Shimo-Shidami, Moriyama-ku, Nagoya 463-8560, Japan; nomura-k@aist.go.jp (K.N.); m-mikami@aist.go.jp (M.M.); y.kinemuchi@aist.go.jp (Y.K.); terra@cc.nagoya-u.ac.jp (I.T.); w.shin@aist.go.jp (W.S.)

² Department of Physics, Nagoya University, Furo-cho, Chuikusa-ku, Nagoya 464-8602, Japan

³ National Institute of Advanced Industrial Science and Technology (AIST), 1-1-1 Higashi, Tsukuba 305-8565, Japan; n-murayama@aist.go.jp

* Correspondence: a.tsuruta@aist.go.jp; Tel.: +81-52-736-7481

Received: 16 August 2018; Accepted: 5 September 2018; Published: 7 September 2018



Abstract: We measured the coefficient of thermal expansion (CTE) of conducting composite ceramics 30 vol.% CuO-mixed $\text{CaCu}_3\text{Ru}_4\text{O}_{12}$ together with $\text{CaCu}_3\text{Ru}_4\text{O}_{12}$ and CuO. Although conducting ceramics tend to show higher CTE values than insulators, and its CTE value does not match with other ceramic materials, the CTE of $\text{CaCu}_3\text{Ru}_4\text{O}_{12}$ ($7\text{--}9 \times 10^{-6}/\text{K}$) was as small as those of insulators such as CuO ($9 \times 10^{-6}/\text{K}$), alumina ($8 \times 10^{-6}/\text{K}$), and other insulating perovskite oxides. We propose that the thermal expansion of $\text{CaCu}_3\text{Ru}_4\text{O}_{12}$ was suppressed by the Cu-O bond at the A-site due to the Jahn–Teller effect. This unusually small CTE of $\text{CaCu}_3\text{Ru}_4\text{O}_{12}$ compared to other conducting oxides plays a vital role enabling successful coating of 30 vol.% CuO-mixed $\text{CaCu}_3\text{Ru}_4\text{O}_{12}$ thick films on alumina substrates, as demonstrated in our previous study.

Keywords: ceramics heater; conducting oxide; perovskite; thermal expansion

1. Introduction

The coefficient of thermal expansion (CTE) and matching the thermal expansion between different materials are important factors when processing brittle ceramic materials that require high sintering temperatures. Currently, in order to use the heat resistance and functions of ceramic materials, devices containing heterogeneous ceramics with ceramic/ceramic or metal/ceramic interfaces have been actively developed using cofiring [1,2], printing [3,4], and coating [5–10] processes in various industrial fields, including energy [11–13], automotive [14,15], and healthcare [16,17]. Since the target ceramic materials are rarely well-sintered at the desired position when sintered with other materials, the thermal expansion needs to be tailored by optimizing the process, adding complementary materials, or controlling the composition of the ceramic [18,19]. In the case of devices using functional materials, such as perovskite oxides with CTE values often higher than those of other oxides, their thermal expansion behavior has been extensively investigated. When the perovskite composition is modified by the addition of other materials for thermal expansion matching, the properties of the original material may be degraded.

We have focused on the conducting oxide $\text{CaCu}_3\text{Ru}_4\text{O}_{12}$ [20–24] as an alternative conducting material to replace Pt in various high-temperature electrical devices, such as gas sensors [16] and solid oxide fuel cells [25], and have studied its physical properties and processing [26,27]. $\text{CaCu}_3\text{Ru}_4\text{O}_{12}$ is an ordered perovskite oxide, the crystal structure of which is shown in the schematic diagram in Figure 1a.

The resistivity is lower than $1 \text{ m}\cdot\Omega\text{cm}$, even at 500°C , and the temperature dependence shows metallic behavior, which is rarely seen in oxides, as shown in Figure 1b (black plot). Although $\text{CaCu}_3\text{Ru}_4\text{O}_{12}$ is difficult to sinter, we overcame this drawback by adding CuO as a sintering additive, which enabled the fabrication of dense bulks and thick films on alumina substrates [26]. The temperature dependences of the resistivity of 20 vol.% CuO-mixed $\text{CaCu}_3\text{Ru}_4\text{O}_{12}$ bulk and thick film are shown in Figure 1b. The thick film showed resistivity as low as the bulk sample. Scanning Electron Microscope (SEM) images of the thick film are shown in Figure 1c–e, where $\text{CaCu}_3\text{Ru}_4\text{O}_{12}$ grains were firmly bound to adjacent $\text{CaCu}_3\text{Ru}_4\text{O}_{12}$ grains and to the alumina substrate without cracks and peeling. Recently, we tried to fabricate a SnO_2 gas sensor using CuO-mixed $\text{CaCu}_3\text{Ru}_4\text{O}_{12}$ thick films as electrodes and heater instead of Pt on an alumina substrate [28]. Our trial successfully showed similar sensing performance as the sensor using Pt. In addition, CuO-mixed $\text{CaCu}_3\text{Ru}_4\text{O}_{12}$ thick film heaters on alumina substrates were robust against thermal shock and rapid thermal cycling.

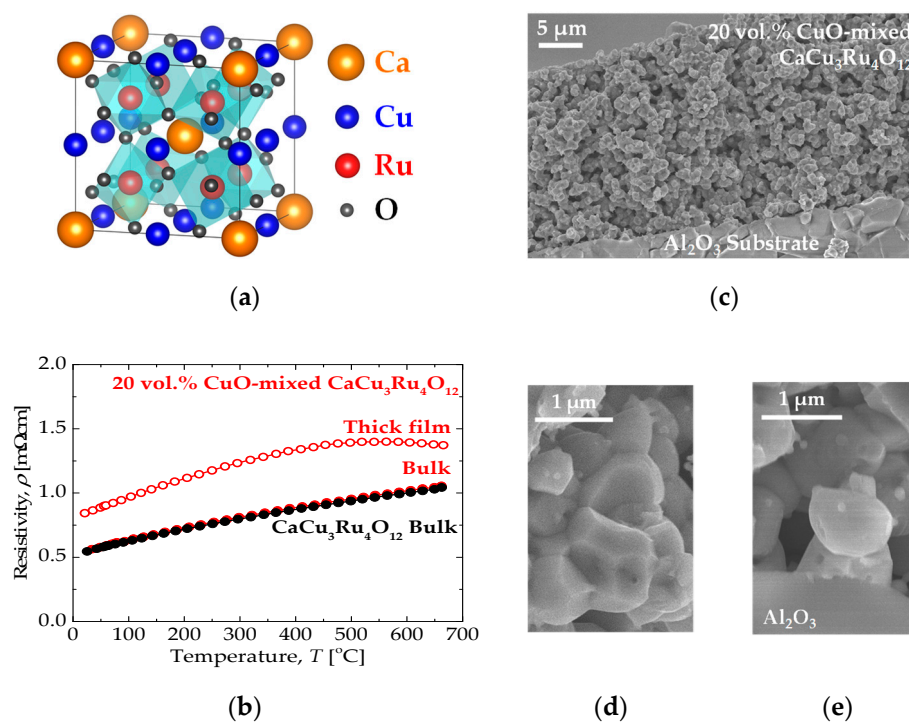


Figure 1. (a) Crystal structure of $\text{CaCu}_3\text{Ru}_4\text{O}_{12}$. (b) Temperature dependence of the resistivity of a $\text{CaCu}_3\text{Ru}_4\text{O}_{12}$ bulk, a 20 vol.% CuO-mixed $\text{CaCu}_3\text{Ru}_4\text{O}_{12}$ bulk, and a 20 vol.% CuO-mixed $\text{CaCu}_3\text{Ru}_4\text{O}_{12}$ thick film. (c) Cross-sectional SEM image of a 20 vol.% CuO-mixed $\text{CaCu}_3\text{Ru}_4\text{O}_{12}$ thick film on an alumina substrate. (d) and (e) are magnified images of the film and the film–substrate interface, respectively, shown in (c).

We observed that $\text{CaCu}_3\text{Ru}_4\text{O}_{12}$ and CuO can be easily compounded, and the composite thick film showed excellent sintering on an alumina substrate without any cracks. We further observed that the thick film heater showed excellent durability against rapid heat cycles. All these findings were truly unexpected for a conventional ceramic device. Hence, in this study, we investigated the thermal expansion of $\text{CaCu}_3\text{Ru}_4\text{O}_{12}$, CuO, and CuO-mixed $\text{CaCu}_3\text{Ru}_4\text{O}_{12}$ in order to clarify the reason for the excellent properties of our ceramic device. In addition, we compared the thermal expansion of $\text{CaCu}_3\text{Ru}_4\text{O}_{12}$ with that of other perovskite oxides.

2. Experimental

$\text{CaCu}_3\text{Ru}_4\text{O}_{12}$ was prepared via a solid-state reaction [22,26,29]. Stoichiometric mixtures of CaCO_3 , CuO, and RuO_2 were pressed into pellets and calcined in air at 1000°C for 48 h. The pellets

were covered by a mixture of excess CaCO_3 , CuO , and RuO_2 powders to prevent Ru sublimation during sintering and subsequent deviations from the desired composition. The $\text{CaCu}_3\text{Ru}_4\text{O}_{12}$ powder was obtained via mechanical grinding and ball-milling of the calcined pellets.

The $\text{CaCu}_3\text{Ru}_4\text{O}_{12}$ powder was then mixed with CuO powder (as a sintering additive), then pressed into a pellet and sintered at $1000\text{ }^\circ\text{C}$ for 48 h in air. The CuO volume fraction in the bulk was 30 vol.% corresponding to 29.5 wt.%. The volume fraction was calculated using the molecular weights and lattice constants of each material. A CuO bulk sample was obtained by calcining a pressed pellet of CuO powder under the same conditions as the 30 vol.% CuO -mixed $\text{CaCu}_3\text{Ru}_4\text{O}_{12}$ bulk sample. The relative densities of the 30 vol.% CuO -mixed $\text{CaCu}_3\text{Ru}_4\text{O}_{12}$ and CuO bulk samples were 73% and 92%, respectively.

X-ray diffraction (XRD) of the $\text{CaCu}_3\text{Ru}_4\text{O}_{12}$ powder was performed using a standard diffractometer with parallel-beam optics of $\text{Cu K}\alpha$ radiation in the 2θ - θ scan mode (X'Pert Pro MPD, Malvern Panalytical, Malvern, UK) at 25, 100, 200, 300, 400, 500, 600, 700, 800, and $900\text{ }^\circ\text{C}$ using a reactor chamber (XRK900, Anton Paar, Graz, Austria) in air [30]. The XRD patterns at all temperatures were analyzed using the Rietveld method [31] and we calculated the lattice constants using the reported space group and crystal structural parameters as the initial value [32]. The CTEs of 30 vol.% CuO -mixed $\text{CaCu}_3\text{Ru}_4\text{O}_{12}$ and CuO bulk samples were measured in air using a thermomechanical analyzer (TMA; Thermo Plus EVO2, Rigaku, Tokyo, Japan).

3. Results and Discussion

Figure 2 shows the XRD pattern for $\text{CaCu}_3\text{Ru}_4\text{O}_{12}$ powder measured at $25\text{ }^\circ\text{C}$. All peaks were well-indexed to those of $\text{CaCu}_3\text{Ru}_4\text{O}_{12}$ [32] and no heterogeneous or impurity phases were identified. Figure 3a shows the lattice constant of $\text{CaCu}_3\text{Ru}_4\text{O}_{12}$ calculated from powder XRD, plotted as a function of temperature. $\text{CaCu}_3\text{Ru}_4\text{O}_{12}$ belongs to a large family of ordered perovskites described by the general formula $\text{AC}_3\text{B}_4\text{O}_{12}$, and can be considered as a fourfold superstructure of the ABO_3 perovskite shown in Figure 1a. The lattice constant increased with increasing temperature, indicating positive thermal expansion, similar to other conventional oxide materials. The plot represents the lattice constant a for the cubic structure, from which the relative thermal expansion and CTE values were evaluated.

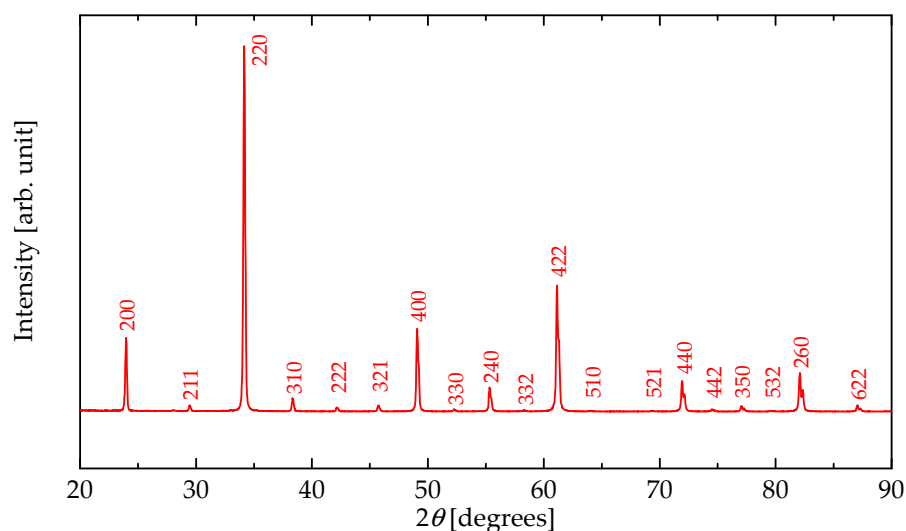


Figure 2. X-ray diffraction (XRD) ($\text{CuK}\alpha$) pattern of $\text{CaCu}_3\text{Ru}_4\text{O}_{12}$ powder measured at $25\text{ }^\circ\text{C}$.

Considering the potential applications of the perovskite, the thermal expansion should be evaluated using TMA. However, here the CTE of $\text{CaCu}_3\text{Ru}_4\text{O}_{12}$ had to be calculated from the lattice constant because $\text{CaCu}_3\text{Ru}_4\text{O}_{12}$ could not be fully sintered. Figure 3b shows the thermal expansion

relative to the value at 25 °C ($\Delta L/L_{25}$) for the 30 vol.% CuO-mixed $\text{CaCu}_3\text{Ru}_4\text{O}_{12}$ and CuO bulk samples measured using TMA, together with that of $\text{CaCu}_3\text{Ru}_4\text{O}_{12}$ calculated from the data shown in Figure 3a. The thermal-expansion curves of $\text{CaCu}_3\text{Ru}_4\text{O}_{12}$ and CuO were nearly identical between 25 °C and 900 °C. Hence, we concluded that the addition of 30 vol.% CuO to $\text{CaCu}_3\text{Ru}_4\text{O}_{12}$ did not significantly affect thermal-expansion behavior, although a detailed analysis was not performed [33]. This good thermal-expansion match is the reason that no serious cracks or exfoliation at the interface between $\text{CaCu}_3\text{Ru}_4\text{O}_{12}$ and CuO were observed in the composite material; this supports the results of our previous study where we successfully used CuO as a sintering additive for $\text{CaCu}_3\text{Ru}_4\text{O}_{12}$ [26].

Figure 3c shows the temperature dependence of the CTE of the 30 vol.% CuO-mixed $\text{CaCu}_3\text{Ru}_4\text{O}_{12}$ bulk, CuO bulk, and $\text{CaCu}_3\text{Ru}_4\text{O}_{12}$ samples. The dotted and broken lines show the CTE at 400 °C of alumina and ZrO_2 , respectively, for comparison, as they are widely used ceramic substrate materials. Although the $\Delta L/L_{25}$ of the three materials were almost the same at all temperatures, the CTEs, which are generally calculated as the differential value of $\Delta L/L_{25}$, were slightly different, especially around room temperature. The CTE curve of the 30 vol.% CuO-mixed $\text{CaCu}_3\text{Ru}_4\text{O}_{12}$ bulk sample was located between those of CuO bulk and $\text{CaCu}_3\text{Ru}_4\text{O}_{12}$ at all temperatures, showing an acceptable average value. The 30 vol.% CuO-mixed $\text{CaCu}_3\text{Ru}_4\text{O}_{12}$ bulk sample showed almost the same CTE value as alumina. Thus, in our previous study, the CuO-mixed $\text{CaCu}_3\text{Ru}_4\text{O}_{12}$ thick film was successfully coated and sintered on alumina substrates without cracking or peeling due to this good CTE match.

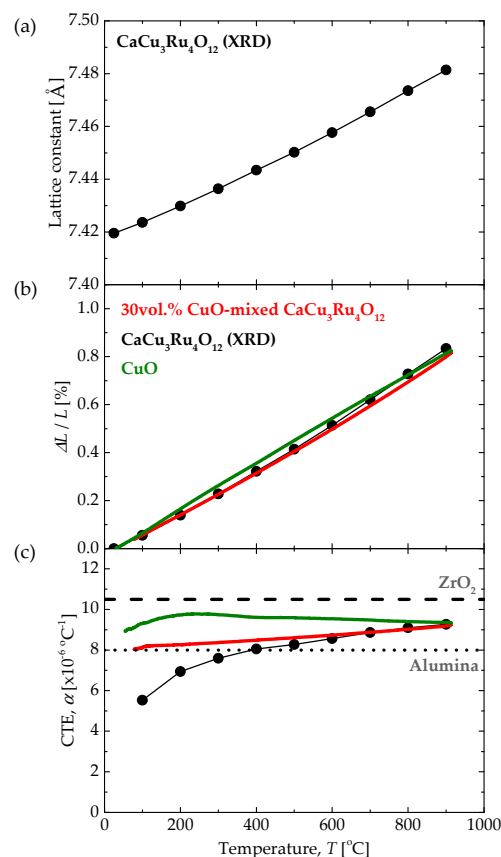


Figure 3. (a) Lattice constant of $\text{CaCu}_3\text{Ru}_4\text{O}_{12}$ as a function of temperature. (b) Temperature dependence of $\Delta L/L_{25}$ and (c) temperature dependence of the CTE of the 30 vol.% CuO-mixed $\text{CaCu}_3\text{Ru}_4\text{O}_{12}$ bulk, CuO bulk, and $\text{CaCu}_3\text{Ru}_4\text{O}_{12}$ samples. Data for the 30 vol.% CuO-mixed $\text{CaCu}_3\text{Ru}_4\text{O}_{12}$ bulk and CuO bulk were measured using a thermomechanical analyzer (TMA), while those for $\text{CaCu}_3\text{Ru}_4\text{O}_{12}$ were calculated from powder XRD.

Inorganic materials have various favorable properties, including conductivity, dielectricity, and magnetism. The CTE (α) depends on such properties, as follows: [34]

$$\alpha = \alpha_{\text{vib}} + \alpha_{\text{elec}} + \alpha_{\text{mag}} + \alpha_{\text{fe}} + \alpha_{\text{vac}} \quad (1)$$

where α_{vib} , α_{elec} , α_{mag} , α_{fe} , and α_{vac} correspond to the CTE due to vibrational, electronic, magnetic, ferroelectric contribution, and vacancy formation, respectively. This formula is derived considering that the CTE is the second derivative of the Gibbs energy, where functional materials have higher energies than materials without these properties. Therefore, α of a simple insulator should be the lowest among ceramic oxide materials, except for ZrW_2O_8 [35] and $\text{LaCu}_3\text{Fe}_4\text{O}_{12}$ [36], which show negative thermal expansion due to peculiar mechanisms, such as lattice bending and valence transitions. Since $\text{CaCu}_3\text{Ru}_4\text{O}_{12}$ shows particularly high electrical conductivity compared to other perovskite oxides, its α_{elec} and α values are expected to be larger than those of other materials.

Let us compare $\text{CaCu}_3\text{Ru}_4\text{O}_{12}$ with other ABO_3 -type oxides; Table 1 shows the CTE, conducting behavior, B-site cation, electron orbital of the B-site cation, and the number of d-electron of various oxides. Here, we focus on simple ABO_3 -type oxides in order to simplify the comparison and discussion. The CTE values were taken directly from the references, or calculated from the temperature dependence of the lattice volume. In this paper, the materials are classified as conductor or insulator using $10 \Omega\text{cm}$ of resistivity at room temperature as a threshold. As expected, the conductors $\text{Sr}_{0.8}\text{La}_{0.2}\text{TiO}_3$, SrRuO_3 , $\text{La}_{0.6}\text{Sr}_{0.4}\text{Fe}_{0.2}\text{Co}_{0.8}\text{O}_{3-x}$, SrCoO_3 , LaCoO_3 , and $\text{LaCo}_{0.5}\text{Ni}_{0.5}\text{O}_3$ show larger CTE values than materials with insulating, ferroelectric, or dielectric properties. However, the CTE of $\text{CaCu}_3\text{Ru}_4\text{O}_{12}$ is remarkably small compared to other conductors. $\text{La}_{0.6}\text{Sr}_{0.4}\text{Fe}_{0.2}\text{Co}_{0.8}\text{O}_{3-x}$, SrCoO_3 , and LaCoO_3 are used as cathode materials in solid oxide fuel cells, and many oxygen vacancies are generated at high temperature; hence, α_{elec} and α_{vac} strongly contribute to α in these materials.

Table 1. CTE, conduction behavior, B-site cation, electron orbital of B-site cation, and number of d-electron of various perovskite oxide.

Material	CTE ($\times 10^{-6}/\text{K}$)	Conduction Behavior	B-Site Cation	Electron Orbital of B-Site Cation	Number of D-Electron
MgTiO_3 [34]	10.1	Insulator	Ti^{4+}	$3d^0$	0
CaTiO_3 [34]	11.6	Insulator	Ti^{4+}	$3d^0$	0
BaTiO_3 [34]	12.1	Insulator	Ti^{4+}	$3d^0$	0
$\text{Sr}_{0.8}\text{La}_{0.2}\text{TiO}_3$ [37]	12.5	Conductor	Ti^{4+}	$3d^0$	0
LiNbO_3 [34]	13.7	Insulator	Nb^{5+}	$4d^0$	0
CaHfO_3 [34]	9.6	Insulator	Hf^{4+}	$5d^0$	0
LiTaO_3 [34]	13.3	Insulator	Ta^{5+}	$5d^0$	0
KTaO_3 [34]	7.01	Insulator	Ta^{5+}	$5d^0$	0
YVO_3 [38]	6.4	Insulator	V^{3+}	$3d^2$	2
LaCrO_3 [34]	9.2	Insulator	Cr^{3+}	$3d^3$	3
YMnO_3 [34]	11.2	Insulator	Mn^{3+}	$3d^4$	4
LaMnO_3 [34]	10.9	Insulator	Mn^{3+}	$3d^4$	4
SrRuO_3 [39]	12.7	Conductor	Ru^{4+}	$4d^4$	4
$\text{CaCu}_3\text{Ru}_4\text{O}_{12}$	8.9	Conductor	Ru^{4+}	$4d^4$	4
LaFeO_3 [34]	9.7	Insulator	Fe^{3+}	$3d^5$	5
$\text{La}_{0.6}\text{Sr}_{0.4}\text{Fe}_{0.2}\text{Co}_{0.8}\text{O}_{3-x}$ [19]	21.4	Conductor	$\text{Fe}^{3+}, \text{Co}^{3+}$	$3d^5, 3d^6$	5.8
SrCoO_3 [34]	15.6	Conductor	Co^{4+}	$3d^5$	5
LaCoO_3 [34]	23.1	Conductor	Co^{3+}	$3d^6$	6
$\text{LaCo}_{0.5}\text{Ni}_{0.5}\text{O}_3$ [40]	15.1	Conductor	$\text{Co}^{3+}, \text{Ni}^{3+}$	$3d^6, 3d^7$	6.5
ErNiO_3 [41]	8.1	Insulator	Ni^{3+}	$3d^7$	7
CaSnO_3 [34]	9.2	Insulator	Sn^{4+}	$4d^{10}$	10

The CTE values are quoted at 500 °C; for the datasets where this value was not stated, the data were linearly extrapolated to 500 °C.

The conduction behavior of the perovskite oxides correlates with the number of d-electrons in the B-site cation. Hence, CTE values are plotted as a function of the number of d-electrons in Figure 4, where the conduction behavior of each material is represented by symbols. The CTE values

of all insulators are located in the lower part of the figure, consistent with the theory expressed by Equation (1). Although the ferroelectric materials, such as BaTiO₃, LiTaO₃ and LiNbO₃, are electrically insulating, they show relatively large CTE values compared to the other insulators because of structural deformations due to polarization. Almost all conductors show CTE values larger than $10 \times 10^{-6}/\text{K}$, where that of CaCu₃Ru₄O₁₂ is surprisingly small, despite of its high electrical conductivity. CaCu₃Ru₄O₁₂ and SrRuO₃ are closely related materials; they both show high conductivity and have Ru occupying the B-site of perovskite. However, the CTE values of these materials are significantly different, where CaCu₃Ru₄O₁₂ has a smaller value than the simple SrRuO₃ perovskite. The structural difference between those materials is that Ca and Cu are ordered at the A-site of the perovskite structure in CaCu₃Ru₄O₁₂. Cu does not usually occupy the A-site because Cu²⁺ normally appears in 6 coordination. However, Cu in CaCu₃Ru₄O₁₂ is stabilized at the A-site owing to the Jahn–Teller effect. CuO octahedra extend in the z-axis direction with separation of the degenerated e_g orbital, while Cu²⁺ acts as a large cation and can occupy the A-site. Cu atoms occupy 75% of the A-site in CaCu₃Ru₄O₁₂, and the Cu–O bond, which is stabilized at lower energy via separation of the degenerated e_g orbital, would be stronger than other simple bonds such as Ca–O and Ru–O. If this Cu–O bond is predominant in the thermal expansion of the CaCu₃Ru₄O₁₂ lattice, the thermal expansion will be similar to that of CuO, as shown in Figure 3b. Such a contribution of the A-site cation to the thermal expansion is a novel feature of ordered perovskite and is a great advantage in material design and applications.

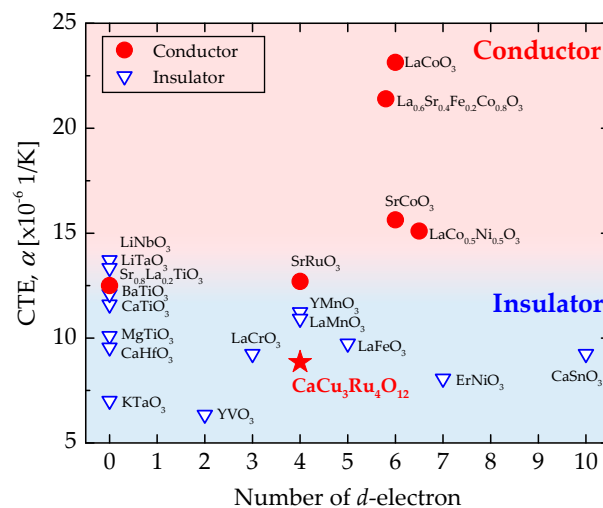


Figure 4. CTE of various perovskite oxides plotted as a function of the number of d-electrons.

Finally, we show the heater characteristics of a 30 vol.% CuO-mixed CaCu₃Ru₄O₁₂ thick-film heater on an alumina substrate realized by the unusually small thermal expansion of CaCu₃Ru₄O₁₂ and CTE matching between CaCu₃Ru₄O₁₂ and alumina. The thick-film heater was fabricated on an alumina substrate ($3.0 \times 25 \times 0.3$ mm) by screen-printing a paste of CuO and CaCu₃Ru₄O₁₂ powders mixed in a suitable vehicle. Figure 5a shows a photograph and a thermal-camera image while 32 V DC voltage was applied to the 30 vol.% CuO-mixed CaCu₃Ru₄O₁₂ thick-film heater. The meandering heater pattern generates heat up to 600 °C due to Joule heating. Figure 5b shows the temperature (T), defined as the maximum temperature over the heater pattern in air as a function of the applied voltage. The temperature increased linearly with applied voltage, expressed as $T = 23.4 V - 146$ in units of degrees Celsius; this linear V - T characteristic indicates good temperature controllability of the heater. The temperature of the heater under 32.0 V pulses, with a width of 10 s and a cycle length of 20 s, is shown in Figure 5c. The temperature increased immediately from room temperature when the voltage was applied, reaching 600 °C within 9 s. The heater temperature followed the cyclic voltage pulses without degradation, and the performance was maintained after many cycles. It is

clear from these results that the 30 vol.% CuO-mixed $\text{CaCu}_3\text{Ru}_4\text{O}_{12}$ thick-film heater on an alumina substrate is surprisingly robust and is thought to be reliable enough to be used as a substitute for Pt as a conducting material for various electrical devices.

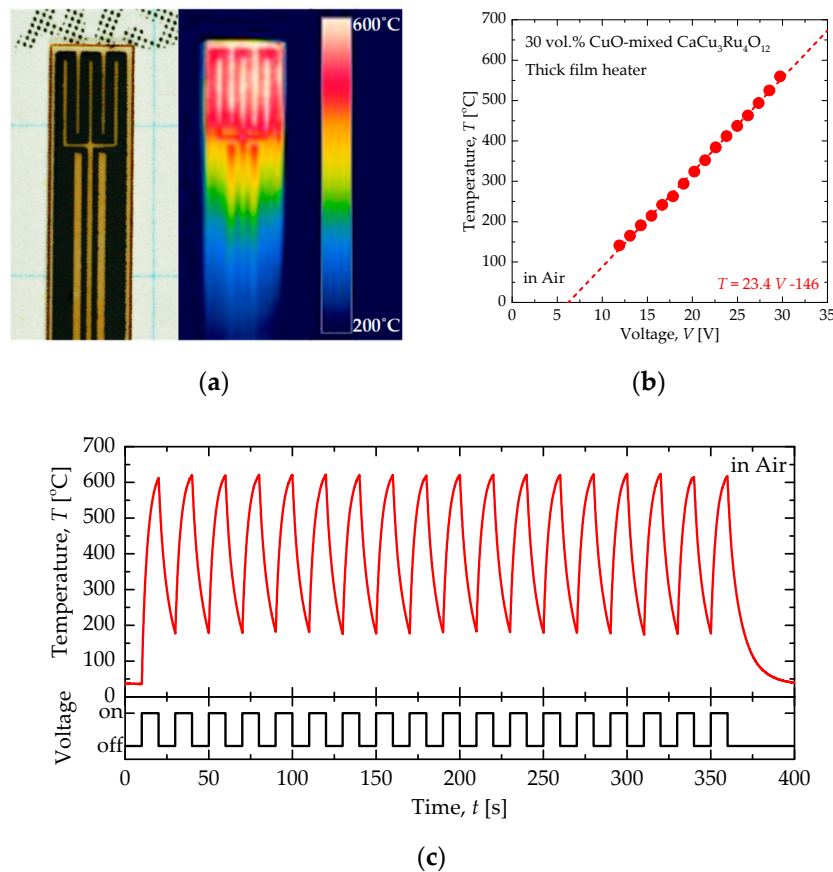


Figure 5. (a) Photograph of the 30 vol.% CuO-mixed $\text{CaCu}_3\text{Ru}_4\text{O}_{12}$ thick-film heater on the alumina substrate and a thermal-camera image with an applied voltage of 32 V DC. (b) Temperature (T), defined as the maximum temperature over the meandering heater pattern, as a function of the applied voltage. (c) Temperature of the heater under cyclic 32.0 V pulses with a width of 10 s and cycle time of 20 s. All experiments were performed in air.

4. Conclusions

We measured the CTE of 30 vol.% CuO-mixed $\text{CaCu}_3\text{Ru}_4\text{O}_{12}$ and CuO bulk samples using TMA and calculated the CTE of $\text{CaCu}_3\text{Ru}_4\text{O}_{12}$ from the lattice constant determined using high-temperature XRD measurements. The $\Delta L/L_{25}$ of these materials were nearly identical between 25 °C and 900 °C; we measured the values for $\text{CaCu}_3\text{Ru}_4\text{O}_{12}$, CuO, and 30 vol.% CuO-mixed $\text{CaCu}_3\text{Ru}_4\text{O}_{12}$ of $8.27 \times 10^{-6} \text{ K}^{-1}$, $9.59 \times 10^{-6} \text{ K}^{-1}$, and $8.60 \times 10^{-6} \text{ K}^{-1}$, respectively, at 500 °C. These values were similar to those of alumina ($8.0 \times 10^{-6} \text{ K}^{-1}$). The CTE matches between $\text{CaCu}_3\text{Ru}_4\text{O}_{12}$ /CuO and 30 vol.% CuO-mixed $\text{CaCu}_3\text{Ru}_4\text{O}_{12}$ /alumina explain the successful compounding and coating of these material pairs demonstrated in our previous study. The CTE of $\text{CaCu}_3\text{Ru}_4\text{O}_{12}$ is smaller than that of other conducting perovskite oxides, and close to the values for insulating perovskite oxides. The unusually small CTE of $\text{CaCu}_3\text{Ru}_4\text{O}_{12}$ is thought to be due to the influence of Cu occupying the A-site of the perovskite via the Jahn–Teller effect. Such a contribution of the A-site cation in the ordered perovskite material to the thermal expansion offers a novel and superior advantage in material design and applications.

Author Contributions: A.T., I.T., and W.S. conceived and designed the experiments; A.T. performed the experiments; K.N. measured and analyzed high-temperature XRD; A.T., I.T., and W.S. analyzed the data; M.M., Y.K., and N.M. helped with the experiments and discussed the results; A.T. wrote the paper.

Funding: This research received no external funding.

Conflicts of Interest: The authors declare no conflict of interest.

References

1. Gongora-Rubio, M.R.; Espinoza-Vallejos, P.; Sola-Laguna, L.; Santiago-Avilés, J.J. Overview of low temperature co-fired ceramics tape technology for meso-system technology (MsST). *Sens. Actuators A* **2001**, *89*, 222–241. [[CrossRef](#)]
2. Miyazaki, H.; Iwakiri, S.; Hirao, K.; Fukuda, S.; Izu, N.; Yoshizawa, Y.; Hyuga, H. Effect of high temperature cycling on both crack formation in ceramics and delamination of copper layers in silicon nitride active metal brazing substrates. *Ceram. Int.* **2017**, *43*, 5080–5088. [[CrossRef](#)]
3. Jean, J.H.; Chang, C.R.; Chen, Z.C. Effect of Densification Mismatch on Camber Development during Cofiring of Nickel-Based Multilayer Ceramic Capacitors. *J. Am. Ceram. Soc.* **1997**, *80*, 2401–2406. [[CrossRef](#)]
4. Niimi, H.; Mihara, K.; Sakabe, Y.; Kuwabara, M. Preparation of Multilayer Semiconducting BaTiO₃ Ceramics Co-Fired with Ni Inner Electrodes. *Jpn. J. Appl. Phys.* **2007**, *46*, 6715–6718. [[CrossRef](#)]
5. Park, J.H.; Akedo, J.; Sato, H. High-speed metal-based optical microscanners using stainless-steel substrate and piezoelectric thick films prepared by aerosol deposition method. *Sens. Actuators A* **2007**, *135*, 86–91. [[CrossRef](#)]
6. Akedo, J.; Lebedev, M. Piezoelectric properties and poling effect of Pb(Zr, Ti)O₃ thick films prepared for microactuators by aerosol deposition. *Appl. Phys. Lett.* **2000**, *77*, 1710–1712. [[CrossRef](#)]
7. Iijima, Y.; Tanabe, N.; Kohno, O.; Ikeno, Y. In-plane aligned YBa₂Cu₃O_{7-x} thin films deposited on polycrystalline metallic substrates. *Appl. Phys. Lett.* **1992**, *60*, 769–771. [[CrossRef](#)]
8. Kakimoto, K.; Iijima, Y.; Saitoh, T. Fabrication of long-Y123 coated conductors by combination of IBAD and PLD. *Physica C* **2003**, *392–396*, 783–789. [[CrossRef](#)]
9. Doi, T.; Hashimoto, M.; Horii, S.; Ichinose, A. Fabrication of YBa₂Cu₃O₇ Superconducting Film on {100}<001> Textured Cu Tape via Conductive Buffer Layers. *Mater. Trans.* **2017**, *58*, 1493–1499. [[CrossRef](#)]
10. Ichinose, A.; Horii, S.; Doi, T. Possibility of the material cost reduction forward developing low-cost 2nd generation superconducting wires. *Jpn. J. Appl. Phys.* **2017**, *56*, 103101. [[CrossRef](#)]
11. Tucker, M.C.; Lau, G.Y.; Jacobson, C.P.; DeJonghe, L.C.; Visco, S.J. Performance of metal-supported SOFCs with infiltrated electrodes. *J. Power Sources* **2007**, *171*, 477–482. [[CrossRef](#)]
12. Tucker, M.C. Progress in metal-supported solid oxide fuel cells: A review. *J. Power Sources* **2010**, *195*, 4570–4582. [[CrossRef](#)]
13. Nagaya, S.; Watanabe, T.; Tamada, T.; Naruse, M.; Kashima, N.; Katagiri, T.; Hirano, N.; Awaji, S.; Oguro, H.; Ishiyama, A. Development of High Strength Pancake Coil With Stress Controlling Structure by REBCO Coated Conductor. *IEEE Trans. Appl. Supercond.* **2013**, *23*, 4601204. [[CrossRef](#)]
14. Gérard, B. Application of thermal spraying in the automobile industry. *Surf. Coat. Technol.* **2006**, *201*, 2028–2031. [[CrossRef](#)]
15. Song, R.G. Hydrogen permeation resistance of plasma-sprayed Al₂O₃ and Al₂O₃-13wt.% TiO₂ ceramic coatings on austenitic. *Surf. Coat. Technol.* **2003**, *168*, 191–194. [[CrossRef](#)]
16. Itoh, T.; Miwa, T.; Tsuruta, A.; Akamatsu, T.; Izu, N.; Shin, W.; Park, J.; Hida, T.; Eda, T.; Setoguchi, Y. Development of an Exhaled Breath Monitoring System with Semiconductive Gas Sensors, a Gas Condenser Unit, and Gas Chromatograph Columns. *Sensors* **2016**, *16*, 1891. [[CrossRef](#)] [[PubMed](#)]
17. Itoh, T.; Nakashima, T.; Akamatsu, T.; Izu, N.; Shin, W. Nonanal gas sensing properties of platinum, palladium, and gold-loaded tin oxide VOCs sensors. *Sens. Actuators B* **2013**, *187*, 135–141. [[CrossRef](#)]
18. Takenaka, K. Negative thermal expansion materials: Technological key for control of thermal expansion. *Sci. Technol. Adv. Mater.* **2012**, *13*, 013001. [[CrossRef](#)] [[PubMed](#)]
19. Ullmann, H.; Trofimenko, N.; Tietz, F.; Stöver, D.; Ahmad-Khanlou, A. Correlation between thermal expansion and oxide ion transport in mixed conducting perovskite-type oxides for SOFC cathodes. *Solid State Ion.* **2000**, *138*, 79–90. [[CrossRef](#)]
20. Labeau, M.; Bochu, B.; Joubert, J.C.; Chenavas, J. Synthèse et caractérisation cristallographique et physique d'une série de composés ACu₃Ru₄O₁₂ de type perovskite. *J. Solid State Chem.* **1980**, *33*, 257–261. [[CrossRef](#)]

21. Subramanian, M.A.; Sleight, A.W. $\text{ACu}_3\text{Ti}_4\text{O}_{12}$ and $\text{ACu}_3\text{Ru}_4\text{O}_{12}$ perovskites: High dielectric constants and valence degeneracy. *Solid State Sci.* **2002**, *4*, 347–351. [[CrossRef](#)]
22. Kobayashi, W.; Terasaki, I.; Takeya, J.; Tsukada, I.; Ando, Y. A Novel Heavy-Fermion State in $\text{CaCu}_3\text{Ru}_4\text{O}_{12}$. *J. Phys. Soc. Jpn.* **2004**, *73*, 2373–2376. [[CrossRef](#)]
23. Tran, T.T.; Takubo, K.; Mizokawa, T.; Kobayashi, W.; Terasaki, I. Electronic structure of $\text{CaCu}_3\text{Ru}_4\text{O}_{12}$ studied by X-ray photoemission spectroscopy. *Phys. Rev. B* **2006**, *73*, 193105. [[CrossRef](#)]
24. Juan, W.R.; Yuan, Z.Y.; Li, W.; Yong, L.; Jing, S.; Rui, X.; Feng, W.J. Growth and characterization of $\text{CaCu}_3\text{Ru}_4\text{O}_{12}$ single crystal. *Chin. Phys. B* **2015**, *24*, 097501. [[CrossRef](#)]
25. Sumi, H.; Yamaguchi, T.; Hamamoto, K.; Suzuki, T.; Fujishiro, Y.; Matsui, T.; Eguchi, K. AC impedance characteristics for anode-supported microtubular solid oxide fuel cells. *Electrochim. Acta* **2012**, *67*, 159–165. [[CrossRef](#)]
26. Tsuruta, A.; Mikami, M.; Kinemuchi, Y.; Terasaki, I.; Murayama, N.; Shin, W. High electrical conductivity of composite ceramics consisting of insulating oxide and ordered perovskite conducting oxide. *Phys. Status Solidi A* **2017**, *214*, 1600968. [[CrossRef](#)]
27. Tsuruta, A.; Mikami, M.; Kinemuchi, Y.; Terasaki, I.; Murayama, N.; Shin, W. Element Strategy Using Ru-Mn Substitution in $\text{CuO-CaCu}_3\text{Ru}_4\text{O}_{12}$ Composite Ceramics with High Electrical Conductivity. *Crystals* **2017**, *7*, 213. [[CrossRef](#)]
28. Tsuruta, A.; Itoh, T.; Mikami, M.; Kinemuchi, Y.; Terasaki, I.; Murayama, N.; Shin, W. Trial of an All-Ceramic SnO_2 Gas Sensor Equipped with $\text{CaCu}_3\text{Ru}_4\text{O}_{12}$ Heater and Electrode. *Materials* **2018**, *11*, 981. [[CrossRef](#)] [[PubMed](#)]
29. Brizé, V.; Lambert, C.A.; Wolfman, J.; Gervais, M.; Gervais, F. Synthesis and microstructural TEM investigation of $\text{CaCu}_3\text{Ru}_4\text{O}_{12}$ ceramic and thin film. *J. Solid State Chem.* **2011**, *184*, 2719–2723. [[CrossRef](#)]
30. Nomura, K. Crystal Structure and Proton Conduction Path of Perovskite-type Oxides by Using a Laboratory X-ray Diffractometer with a Parallel Beam Optics. *J. Cryst. Soc. Jpn.* **2008**, *50*, 155–160. [[CrossRef](#)]
31. Izumi, F.; Momma, K. Three-dimensional visualization in powder diffraction. *Solid State Phenom.* **2007**, *130*, 15–20. [[CrossRef](#)]
32. Ebbimghaus, S.G.; Weidenkaff, A.; Cava, R.J. Structural Investigations of $\text{ACu}_3\text{Ru}_4\text{O}_{12}$ (A = Na, Ca, Sr, La, Nd)—A Comparison between XRD-Rietveld and EXAFS Results. *J. Solid State Chem.* **2002**, *167*, 126–136. [[CrossRef](#)]
33. Rosen, B.W.; Hashin, Z. Effective thermal expansion coefficients and specific heats of composite materials. *Int. J. Eng. Sci.* **1970**, *8*, 157–173. [[CrossRef](#)]
34. Inaba, H.; Tagawa, H. Semi-Empirical Estimation of Thermal Expansion Coefficients of Perovskite-Type Oxides. *J. Ceram. Soc. Jpn.* **1998**, *106*, 272–278. [[CrossRef](#)]
35. Mary, T.A.; Evans, J.S.O.; Vogt, T.; Sleight, A.W. Negative Thermal Expansion from 0.3 to 1050 Kelvin in ZrW_2O_8 . *Science* **1996**, *272*, 90–92. [[CrossRef](#)]
36. Long, Y.W.; Hayashi, N.; Saito, T.; Azuma, M.; Muranaka, S.; Shimakawa, Y. Temperature-induced A–B intersite charge transfer in an A-site-ordered $\text{LaCu}_3\text{Fe}_4\text{O}_{12}$ perovskite. *Nature* **2009**, *458*, 60–63. [[CrossRef](#)] [[PubMed](#)]
37. Park, B.; Lee, J.; Lee, S.; Lim, T.; Park, S.; Snog, R.; Im, W.B.; Shin, D. La-doped SrTiO_3 interconnect materials for anode-supported flat-tubular solid oxide fuel cells. *Int. J. Hydrogen Energy* **2012**, *37*, 4319–4327. [[CrossRef](#)]
38. Blake, G.R.; Palstra, T.T.M.; Ren, Y.; Nugroho, A.A.; Menovsky, A.A. Neutron diffraction, x-ray diffraction, and specific heat studies of orbital ordering in YVO_3 . *Phys. Rev. B* **2002**, *65*, 174112. [[CrossRef](#)]
39. Kennedy, B.J.; Hunter, B.A. High-temperature phases of SrRuO_3 . *Phys. Rev. B* **1998**, *58*, 653. [[CrossRef](#)]
40. Wang, X.; Han, Y.; Song, X.; Liu, W.; Jin, Y.; Liu, W.; Cui, H. An insight into the effects of transition metals on the thermal expansion of complex perovskite compounds: An experimental and density functional theory investigation. *Phys. Chem. Chem. Phys.* **2018**, *20*, 17781–17789. [[CrossRef](#)] [[PubMed](#)]
41. Alonso, J.A.; Martínez-Lope, M.J.; Casais, M.T.; García-Muñoz, J.L.; Fernández-Díaz, M.T.; Aranda, M.A.G. High-temperature structural evolution of RNiO_3 (R = Ho, Y, Er, Lu) perovskites: Change disproportionation and electronic localization. *Phys. Rev. B* **2001**, *64*, 094102. [[CrossRef](#)]

